The effect of pressure on structural, stability, electronic, and optical properties of hydrogenated silicene: A first-principle study

V Kumar (vkumar52@hotmail.com)
Indian School of Mines

R. Santosh
IITISM: Indian Institute of Technology

Research Article

Keywords: hydrogenated silicene, pressure, stability and energy bandgap

Posted Date: March 26th, 2021

DOI: https://doi.org/10.21203/rs.3.rs-318962/v1

The effect of pressure on structural, stability, electronic, and optical properties of hydrogenated silicene: A first-principle study

V. Kumar*, R. Santosh,
Department of Electronics Engineering,
Indian Institute of Technology (Indian School of Mines), Dhanbad 826004, India.
*Corresponding author. E-mail address: vkumar52@hotmail.com.

ABSTRACT

The structural, electronic, and optical properties of hydrogenated silicene have been studied under different pressures using first-principle calculations. The binding energy and band structure have been calculated for two stable structures: Chair (C-) and Boat (B-) in the range of 0-21 GPa external pressure. The behavior of stability and energy bandgap have been analyzed under different external pressures. The stability has been verified using binding energy and phonon data. The C- and B- structures have zero bandgaps at 21 GPa and become unstable. The optical properties of B-configuration have been studied in the energy range of 0-20 eV. Five optical parameters such as conductivity threshold (σ_{th}), dielectric constant $\varepsilon(0)$, refractive index $n(0)$, birefringence $\Delta n(0)$ and plasmon energy ($\hbar\omega_p$) have been calculated for the first time under different pressures. The calculated values are in good agreement with the reported values at 0 GPa.

---

1 Introduction

In the last decade, increasing interest has been given to the study of two-dimensional graphene due to its exceptional properties such as high carrier mobility, current carrying capacity, non-zero berry's phase, unusual quantum Hall effect, linear dispersion energy bands, etc [1-3]. However, graphene may not be compatible with the present silicon technology and

integrated circuits. Accordingly, researchers investigated the other IVA group elements, such as silicene and germanene. Silicene and Germanene are the graphene analogy of silicon and germanium. Silicon is the more abundant element compared to germanium, and also silicene has exceptional properties such as linear dispersing energy bands, massless Dirac distribution, and quantum Hall effect [4-6] ferromagnetic [7], half metallicity [8], giant magneto resistance[9], and superconductivity properties [10]. It exhibits good spin-orbit coupling, a spin-orbit gap at Dirac points [11], the emergence of valley polarized metal phase for spintronic applications [12, 13]. Silicene has zero energy bandgap like graphene and also has less thermal conductivity [14, 15]. To introduce the energy band gap many procedures have been used such as chemical functionality [16,17], application of electric field [18], doping [19], substrate effect [20], nanoribbon [21,22], and introducing nanoholes [23,24]. Hydrogenation is a well-known technique to creates a bandgap and increases the thermal conductivity of silicene [25, 26]. The hydrogenated silicene is normally referred to as silicane, which is experimentally observed on Ag (111) [27-28]. The silicane is stable up to 450 K temperature, and after that, dehydration occurs, and the surface restores initial silicene [29].

Several researchers have performed first-principle calculations to study the structural, electronic, magnetic, and thermal properties of hydrogenated silicene [30-35]. Lui et al. [36] have calculated the thermal properties of silicane and predicted that hydrogenation leads to a large increment of thermal conductivity from 22.5 $Wm^{-1}K^{-1}$ to 78.0 $Wm^{-1}K^{-1}$. The effect of hydrogen in the silicene sheet has been studied in which half-silicane shows ferromagnetic behavior [37]. Nguyen et al. [38] have studied the hydrogenated silicene and graphene that confirms silicene has a strong binding with hydrogen compared to graphene. Some researchers calculated the carrier mobility and electron transport properties of silicene and hydrogenated

silicene [39-41]. Molecular dynamics simulation reveals the stability of adsorption configurations of hydrogenated silicene [42].

Some researchers have reported the hydrogenation of silicene for different structures [25, 26] out of which chair (C-), boat (B-) structures are most stable. Recently, the authors[43-45] have studied the several properties of hydrogenated graphene, hydrogenated silicene, and hydrogenated germanene using first-principle calculations. The authors have also have studied the pressure effect on the various properties of functionalized graphene and germanene [46-48]. Till now, no work has been carried out on the properties of C- and B- structures of hydrogenated silicene under different pressures. Therefore, we thought it would be of interest to study the structural, electronic, and optical properties of C- and B- conformers of hydrogenated silicene under external pressures.

In this paper, first-principle calculations have used to calculate the lattice constants (a, b, and c), bond lengths ($d_{Si\text{-}Si}$ and $d_{Si\text{-}H}$), bond angles ($\theta_{Si\text{-}Si\text{-}Si}$ and $\theta_{Si\text{-}Si\text{-}H}$), energy bandgap ($E_g$), and binding energy ($E_b$) in the pressure range of 0 GPa - 21 GPa. The stability has been analyzed using the binding energy and phonon calculations. The behavior of the energy bandgap has been studied for every 3 GPa rise in external pressures. The optical parameters of B-configuration such as (σ_{th}), $\varepsilon(0)$, $n(0)$, $\Delta n(0)$ and $\hbar\omega_p$ have been calculated in in-plane ($E \perp c$) and out of plane ($E \| c$) polarization for the first time.

2 Methodology

The calculations have been performed using the Cambridge Sequential Total Energy Package (CASTEP) code [49]. The generalized gradient approximation (GGA) has been used with the Perdew-Burke-Ernzerhof scheme (PBE) [50-52]. A plane-wave basis set kinetic energy cut-off

of 272 eV has been used in an ultra-soft Pseudopotential representation in reciprocal crystal lattice [53]. The optimized structure has been obtained by applying the Broyden, Fletcher, Goldfarb, and Shanno BFGS scheme [54]. Throughout the optimization of geometry, maximum tolerance of total energy convergence of 0.2×10^{-4} eV/atom, Fermi energy convergence of $0 .27 \times 10^{-13}$ eV, Hellmann–Feynman ionic force of 0.05 eV/Å, maximum stress component 0.1 GPa, and ionic displacement of $0 .2 \times 10^{-2}$ Å have been used.

3. Results and discussion

3.1. Structural and Electronic properties

The hydrogenation of silicene leads to disrupt the π-bonding of adjacent p_z orbitals of silicon atoms. The hexagonal sp^2 hybridized silicene lattice changes to tetrahedral sp^3 hybridized silicane (hydrogenated silicene) with strong σ-bonding. It results in an increase in perpendicular distance between A-type and B-type silicon sub-lattices, which increases the lattice constant and bond lengths. The hydrogenation of silicene forms many structures out of which chair (C-) and boat (B-) structures are the most stable structures [25, 26]. The perspective view of C-silicane is shown in Fig. 1(a). The C-silicane belongs to a space group of P-3M1, which is a trigonal structure having lattice constants of 3.857 Å, 3.857 Å, and 4.59 Å for a, b and c, respectively. The B-silicane belongs to the orthorhombic structure having a space group of PMMN. The perspective view of B-silicane is shown in Fig. 1(b). The optimized lattice parameters are 6.271 Å, 3.714 Å, and 6.015 Å. The calculated bond lengths ($d_{Si\text{-}Si}$ and $d_{Si\text{-}H}$) and bond angles ($\theta_{Si\text{-}Si\text{-}Si}$ and $\theta_{Si\text{-}Si\text{-}H}$) are listed in Table 1 for C-configuration and in Table 2 for B-configuration. There are two pairs of Si-Si bond lengths in B-configuration, one is parallel to the plane, and the other is perpendicular to the plane, which is bonded with hydrogen. The first bond length has a high

value compared to the second due to H-H repulsion [55]. The bond length ($d_{Si\text{-}Si}$) of two configurations of hydrogenated silicene shows a higher value compared to pristine silicene due to the depopulation of bonding orbitals of silicon atoms. This depopulation is due to the electronegativity difference between hydrogen and silicon atoms. The calculated values of structural parameters are in good agreement with the available reported values. The two structures have been optimized for 100 iterations, and the estimated total energies for C- and B-configurations are -247.30 eV and -494.45 eV, respectively. The corresponding Pseudo atomic total energies of Si and H are -165.0639 eV and -12.3526 eV. The binding energy has been calculated using the relation given by Sahin et al. [56, 57], i.e., $E_b = (n_H \times E_T^H + E_T^{Sil} - E_T^{SiH})/n$, where $E_T^H, E_T^{Si}, E_T^{Sil}$ and E_T^{SiH} are the total energies of hydrogen, silicon, silicene, and hydrogenated silicon, respectively, and n_H, n_{Si} n, and N are the number of hydrogen, silicon, the foreign, and a total number of atoms per unit cell, respectively. The calculated E_b shows that the C- and B- configurations have good stability. The positive phonon dispersion confirms the stability of hydrogenated silicene. The atomic populations have been calculated using Mulliken analysis [58] given elsewhere [44].

The nature of the bond has been verified using the bond population. The high value of the bond population confirms the nature of the covalent bond; the medium is semi-ionic and the low value approves ionic bond. The spilling parameter has been calculated using the relation $\sigma = \frac{1}{N_\alpha}\sum_k w_k \sum_\alpha(\psi_\alpha(k)|1 - p(k)|\psi_\alpha(k))$, where N_α is the number of PW states, $\psi_\alpha(k)$ is the Eigen states obtained for given wave vector k, $p(k)$ is the projection operator of Bloch functions with wave vector k. In C-silicane, the calculated bond population of Si-H is 0.82, which conveys the covalent bond, and charge transfer from silicon to hydrogen is 0.08. The value of the spilling parameter for charge and bond population is 1.46% and 13.22%. In B-configuration, the charge

transfer from silicon to hydrogen is 0.08, and the bond population for S-H is 0.86. The value of the spilling parameter for charge transfer and bond population is 1.39% and 6.34%, respectively.

The band structure of hydrogenated silicene has been calculated along with the high symmetry points for two structures and shown in Figs. 2(a) and 2(b). The C-silicane shows an indirect bandgap while the B-configuration has a direct bandgap. The calculated values of the energy gap are listed in Table 1 and Table 2, along with the reported values. A fairly good agreement has been obtained between them. The density of states (DOS) shows the orbital character in the formation of energy bands and states of hybridization. The total density of states (TDOS) and partial density of states (PDOS) have been calculated and shown in Figs. 3(a) and 3(b). The explanation for the density of states of C-configuration has been given in previous publication [44], and for B-configuration, the valence band is divided into three parts. The first part from -11.25 eV to -8.12 eV is mainly influenced by Si-s orbital. The second part from -8.13 eV to -5.27 eV is predominantly influenced by Si-s and H-1s orbitals. The last part from -5.28 eV to Fermi level, is dominated by Si-p and H-s states. The conduction band is the combination of H-s, Si-s, and Si-p orbitals. The hybridization of H-1s and S-3p orbitals plays a major role in the creation of an energy band gap between valence and conduction bands.

Pressure effect on structural and electronic properties

The behavior of structural and electronic properties under different pressures has been studied for C- and B- configurations. The calculated values of lattice constants, bond lengths, bond angles, total energy, unit cell volume, energy bandgap, and binding energy have been listed in Table 1 for C-structure under different pressures from 0 to 21 GPa, and in Table 2 for B-conformer from 0 GPa to 21 GPa. The value of binding energy shows that the stability decreases with the increase of external pressures. The negative value of E_b shows that C- and B-

configurations are unstable at 21 GPa external pressure. The above statement is verified by the phonon calculation in which imaginary frequencies (ω^2 (k, j<0)), shown as negative values below the zero level. These negative values are called soft modes. The soft modes that occur at K-point confirm instability. Table 1 shows the indirect bandgap of C-conformer decreases for every 3 GPa rise in pressure and becomes zero at 21 GPa, whereas for B- configuration, the bandgap becomes zero at 21 GPa.

3.2. Optical properties

The dielectric function is the important parameter in optical properties in which the imaginary part conveys the transitions from occupied electronic states to unoccupied conduction states. The transitions are mainly divided into two: (1) direct and (2) indirect. The direct transitions are further divided into intra-band and inter-band transitions. The intra-band transitions are considered using Drude's contribution with a damping factor δ=0.5 eV, which affects the infrared part of the spectrum. The inter-band transitions are calculated using momentum matrix elements between the valence and conduction band wave functions. The $\varepsilon_2(\omega)$ and momentum matrix elements are calculated using the relation given by Momida et al. [59]. The C- configuration shows an indirect bandgap, which is not suitable for optoelectronic applications. The optical properties of B-configuration have been calculated along the in-plane (E⊥c) and out-of-plane polarization (E||c). The behavior of $\varepsilon_2(\omega)$ of B-configuration is plotted in Figs. 4(a) and 4(b) for E⊥c and E||c planes, respectively, in the energy range of 0-20 eV. The conduction starts at threshold energy (E_{th}) of 2.205 eV in the in-plane polarization and rises rapidly due to more transitions from occupied to unoccupied electronic states. It reaches a maximum value at 4.113 eV due to transitions from the highest occupied valence band (HOVB) of H-1s states to the lowest unoccupied conduction band (LUCB) of Si-3p states. The calculated

optical band gap or conductivity threshold (E_{th}) is listed in Table 3 in which it decreases with an increase of external pressure. The peak value increases under high pressures due to an increase in the range of band structure. In out-of-plane polarization, the conduction starts at 3.646 eV and reaches a maximum value at 6.883 eV. The optical band gap also decreases with the increase of pressure from 0 GPa to 6 GPa and 6 GPa to 12 GPa. The real part of the dielectric function has been calculated using the Kramer-Kronig relation [60] and shown in Figs. 5(a) and 5(b). The calculated dielectric constant in in-plane and out-of-plane polarizations have been listed in Table 3. The calculated value of ε(0) shows the hydrogenation increases the mobility of electrons in pristine silicene. The ε(0) increases with the increase of external pressure, which is due to a decrease in the optical bandgap of the material. Using the Penn model [61], the dielectric constant is inversely proportional to bandgap energy $\varepsilon(0) = 1 + \frac{\hbar\omega_p}{E_g^2}$. The refractive index n(ω) has been derived using the relation given by Sahin et al. [62]. The calculated n(ω) has been shown in Figs.6(a) and 6(b) for E⊥c and E||c under different external pressures: 0 GPa, 6 GPa, and 12 GPa, respectively. The static refractive index in in-plane and out-of-plane polarization are 2.472 and 1.962 respectively and reach maximum values of 3.849 and 3.273 in the mid UV region. The refractive index under different pressures has been listed in Table 3, which increases with the increase of external pressures. The birefringence is the difference between the refractive index in different directions and the calculated birefringence shown in Fig. 7. In the mid UV region, hydrogenated silicene shows large birefringence and the phase-matching condition is no longer satisfied. The electron energy loss function L(ω) has been calculated in both directions using the relation Sahin et al.[62] and shown in Figs. 8(a) and 8(b). The hydrogenated silicene shows high Plasmon energies compared to pristine silicene due to the Π to σ bond translation,

which causes transitions from the lowest occupied valence band to the highest unoccupied conduction band (σ-σ^* plasmons).

4. Conclusions

The behavior of lattice constants, bond lengths, bond angles, energy band gap, total energy, unit cell volume, binding energy has been successfully studied using first-principles from 0 GPa to 21 GPa external pressures. The density of states has been calculated for B-configuration in which H-1s and Si-3p states play a major role in the creation of the energy bandgap. The C-configuration shows an indirect bandgap, and B- the structure has a direct bandgap. Table 1 and Table 2 shows the energy bandgap for two structures decreases with an increase in external pressure and becomes metallic at 21 GPa external pressure. The stability also decreases with the increase of pressure and becomes unstable at 21 GPa. The stability has been verified using binding energy and phonon calculations. Table 3 shows the optical band gap of B-structure decreases with the increase of external pressure in in-plane and out of plane polarization. The functionalization increases the mobility of electrons in pristine silicene. The value of ε(0) increases with the increase of external pressure due to the relation given by Penn et al. hydrogenated silicene has high plasmon energy compared to pristine silicene due to pi to sigma bond translations causes the transitions from the lower part of the valence band to the higher part of the conduction band ((σ-σ^* Plasmons). The $\hbar\omega_p$ of hydrogenated silicene increases with the increase of pressure due to an increase in the range of band structure. The optical parameters such as conductivity threshold (E_{th}), static dielectric constant ε(0), static refractive index n(0), birefringence Δn(0) and Plasmon energy ($\hbar\omega_p$) have been calculated for the first time. The knowledge of these parameters is important in designing of various optoelectronic devices and integrated circuits.

Acknowledgment

The authors are thankful to Ms. Bharthi Gajendra for some calculations and helping with the preparation of the manuscript.

REFERENCES

1. Novosolov, K.S., Geim, A.K., Morozov, S.V., Jiang, D., Zhang, Y., Dubonos, S.V., Grigorieva, I.V., Firsov, A.A.: Electric field effect in atomically thin carbon films. Science 306, 666–669 (2004)
2. Yu, J., Liu, G., Sumant, A.V., Goyal, V., Balandin, A.A.: Graphene-on-diamond devices with increased current-carrying capacity: carbon sp^2-on-sp^3 technology. Nano Lett. 12, 1603–1608 (2012)
3. Zhang, Y., Tan, Y.W., Stomer, H.L., Kim, P.: Experimental observation of the quantum Hall effect and Berry's phase in graphene. Nature 438, 201–204 (2005)
4. Cahangirov, S., Topsakal, M., Aktu, E., Ciraci, S.: Two-dimensional silicon crystals with sizable band gaps and ultrahigh carrier mobility. Phys. Rev, Lett. **236804,** 1–4 (2009).
5. Zhuo, Z., Wu, X., Yang, J.: Two-dimensional silicon crystals with sizable band gaps and ultrahigh carrier mobility. Nanoscale. **10,** 1265-1271 (2018),
6. Liu, C.C., Feng, W., Yao, Y.: Quantum Spin Hall Effect in Silicene and Two-Dimensional Germanium. Phys. Rev. Lett. **107,** 076802 (2011).
7. X.Q. Wang, H.D. Li, J.T. Wang Induced ferromagnetism in one-side semihydrogenated silicene and germanene Phys. Chem. Chem. Phys., 14 (2012), pp. 3031-3036
8. F.-B. Zheng, C.-W. Zhang The electronic and magnetic properties of functionalized silicene: a first-principles study Nanoscale Res. Lett., 7 (2012), p. 422 9. C.-C. Liu, W.

Feng, Y. YaoQuantum spin Hall effect in silicene and two-dimensional germanium Phys. Rev. Lett., 107 (2011), p. 076802

9. C. Xu, G. Luo, Q. Liu, J. Zheng, Z. Zhang, S. Nagase, Z. Gao, J. LuGiant magnetoresistance in silicene nanoribbons Nanoscale, 4 (2012), pp. 3111-3117
10. L. Chen, B. Feng, K. Wu Observation of a possible superconducting gap in silicene on Ag (111) surface Appl. Phys. Lett., 102 (2013), p. 081602
11. Liu, C.C., Jiang, H., Yao, Y.: Low-energy effective Hamiltonian involving spin-orbit coupling in silicene and two-dimensional germanium and tin. Phys. Rev. B **84,** 195430 (2011).
12. Ezawa, M.: Valley-Polarized Metals and Quantum Anomalous Hall Effect in Silicene. Phys. Rev. Lett. **109,** 055502 (2012).
13. Wang, Y., Zheng, J., Ni, Z., Fei, R., Liu, Q., Quhe, R., Chengyong, X., Zhou, J., Zhengxiang G., Lu J.: half-metallic silicene and germanene nanoribbons: towards high-performance spintronics device. Nano **7**,1250037 (2012).
14. Jose, D., Datta, A.: Structures and Chemical Properties of Silicene: Unlike Graphene. Acc. Chem. Res. **47,** 593 (2013).
15. Balendhran, S., Walia, S., Nili, H., Sriram, S., Bhaskaran, M.: Elemental Analogues of Graphene: Silicene, Germanene, Stanene, and Phosphorene. Small **11,** 640 (2015).
16. N. Gao, W.T. Zheng, Q. JiangDensity functional theory calculations for two-dimensional silicene with halogen functionalization Phys. Chem. Chem. Phys., 14 (2012), pp. 257-261
17. S.M. Aghaei, M.M. Monshi, I. Torres, I. CalizoEdge functionalization and doping effects on the stability, electronic and magnetic properties of silicene nanoribbons RSC Adv., 6 (2016), pp. 17046-17058

18. W.F. Tsai, C.-Y. Huang, T.-R. Chang, H. Lin, H.-T. Jeng, A. BansilGated silicene as a tunable source of nearly 100% spin-polarized electrons Nat. Commun., 4 (2013), p. 1500
19. A.Lopez-BezanillaSubstitutional doping widens silicene gap J. Phys. Chem. C, 118 (2014), pp. 18788-18792
20. N. Gao, J. Li, Q. JiangBandgap opening in silicene: Effect of substrates Chem. Phys. Lett., 592 (2014), pp. 222-226
21. Z. Ni, Q. Liu, K. Tang, J. Zheng, J. Zhou, R. Qin, Z. Gao, D. Yu, J. LuTunable bandgap in silicene and germanene Nano Lett., 12 (2011), pp. 113-118
22. Y. Ding, J. NiElectronic structures of silicon nanoribbons Appl. Phys. Lett., 95 (2009), p. 083115
23. F. Pan, Y. Wang, K. Jiang, Z. Ni, J. Ma, J. Zheng, R. Quhe, J. Shi, J. Yang, C. ChenSilicene nanomesh Sci. Rep., 5 (2015), p. 9075.
24. S.M. Aghaei, I. CalizoBand gap tuning of armchair silicene nanoribbons using periodic hexagonal holes J. Appl. Phys., 118 (2015), p. 104304.
25. Houssa, M., Pourtois, G., Heyns, M., Afanas, V., Stesmans, A.: Electronic Properties of Silicene: Insights from First-Principles Modeling. J. Electrochem. Soc. **158,** 185-193 (2011).
26. Fang, D.Q., Zhang, S.L., Xu, H.: Tuning the electronic and magnetic properties of zigzag silicene nanoribbons by edge hydrogenation and doping. RSC Adv. **3,** 24075 (2013).
27. Qiu, J., Fu, H., Xu, Y., Zhou, Q., Meng, S., Li, H., Chen, L., Wu, K.: From Silicene to Half-Silicane by Hydrogenation. ACS Nano **9,** 11192 (2015).
28. Wang, W., Olovsson, W., Uhrberg, R.I.G.: Band structure of hydrogenated silicene on Ag(111): Evidence for half-silicane. Phys. Rev. B **93,** 081406 (2016).

29. Qiu, J., Fu, H., Xu, Y., Oreshkin, A. I., Shao, T., Li, H., Meng, S., Chen, L., Wu, K.: Ordered and Reversible Hydrogenation of Silicene. Phys. Rev. Lett. **114,** 126101 (2015).
30. Voon, L.C.L.Y., Sandberg, E., Aga, R.S., Farajian, A.A.: Hydrogen compounds of group-IV nanosheets. Appl. Phys. Lett. **97,** 163114 (2010).
31. Houssa, M., Scalise, E., Sankaran, K., Pourtois, G., Afanas, V. V., Stesmans, A.: Electronic properties of hydrogenated silicene and germanene. Appl. Phys. Lett. **98,** 223107 (2011).
32. Ju, W., Li, T., , Hou, Z., Wang, H., Cui, H., Li, X., Exotic d^0 magnetism in partial hydrogenated silicene Appl. Phys. Lett. 108 (2016) 212403.
33. Monterola, E.D., Paylag, N.T., Paylag, G.J., Bantaculo, R.V.: Anomalous Effect on the Phononic Thermal Conductivity of Silicene Nanoribbon by Hydrogenation. Adv. Mater. Res. **1105,** 110-114 (2015).
34. Ju, W., Li, T., Su, X., Cui, H., Li, H.: Engineering magnetism and electronic properties of silicene by changing adsorption coverage. Appl. Surf. Sci. **384,** 65–72 (2016).
35. Hussain, T., Kaewmaraya, T., Chakraborty, S., Ahuja, R.: Enhancement of energy storage capacity of Mg functionalized silicene and silicane under external strain. Phys.Chem. Chem. Phys. **15,** 18900 (2013).
36. Liu, Z., Wu, X., Luo, T.: The impact of hydrogenation on the thermal transport of silicone. 2D Mater. **4,** 025002 (2017).
37. Zhang, P., Li, X.D., Hu, C.H., Wu S.Q., Zhu, Z.Z.: First-principles studies of the hydrogenation effects in silicene sheets. Phys. Lett. A **376,** 1230–1233 (2012).
38. Nguyen, M.T., Phong, P.N., Tuyen, N.D.: Hydrogenated Graphene and Hydrogenated Silicene: Computational Insights. Chem. Phys. Chem. **16,** 1733 – 1738 (2015).

39. Fischetti, M.V., Vandenberghe, W.G.: Mermin-Wagner theorem, flexural modes, and degraded carrier mobility in two-dimensional crystals with broken horizontal mirror symmetry. Phys. Rev. B, **93**, 15, 155413 (2016).
40. Gaddemane, G., Vandenberghe, W.G., Van De Put, M.L., Chen, E., Fischetti, M.V.: Monte-Carlo study of electronic transport in non-σh-symmetric two-dimensional materials: Silicene and germanene. J. Appl. Phys., v **124**, 044306 (2018).
41. Khatami, M.M., Gaddemane, G., Van De Put, M.L., Fischetti, M.V., Moravvej-Farshi M.K., Pourfath, M., Vandenberghe, W.G.: Electronic Transport Properties of Silicane Determined from First Principles. Materials, **12**, 2935 (2019).
42. Osborn, T. H., Farajian, A.A., Pupysheva, O.V., Aga, R.S., Voon, L.C.L.Y.: Tunable gaps and enhanced mobilities in strain-engineered silicane. Chem. Phys. Lett. **511**, 101–105 (2011).
43. Kumar, V., Santosh, R., Chandra, S.: First-principle calculations of structural, electronic, optical and thermal properties of hydrogenated graphene. Mat. Sci. & Engg. B **226**, 64-71 (2017).
44. Santosh, R., Kumar, V.: A first-principles study of the stability and structural, optical, and thermodynamic properties of hydrogenated silicene. J. Comp. Elect. **19**, 516-528 (2020).
45. Santosh, R., Sinha, Anita, Kumar V.: Structural, electronic, optical and thermodynamic properties of hydrogenated germanene using first-principle calculations. J. Mat. Sci and Engg. B , Elsevier 259, 114584 **(2020).**
46. Santosh, R., Kumar, V., The structural, electronic, optical and thermodynamical properties of hydrofluorinated graphene: First-principle calculations. Sol. Stat. Sci. 94

70–76 (2019).

47. R. Santosh, V. Kumar, “The effect of pressure on structural, electronic and optical properties of hydrogenated graphene”, J. Computational Electronics, Springer, 18 (3) (2019) 770-778. DOI. 10.1007/s10825-019-01347-x.
48. R. Santosh, V. Kumar, “Structural, electronic, optical and thermodynamic properties of hydrochlorinated graphene: A first-principle study”, J. Molecular Modeling, Springer 25 (2019) 296.
49. Segall, M.D., Philip, J.D., Lindan, M.J., Probert, C.J., Pickard, P.J., Hasnip, S., Clark, J., Payne, M.C.: First-principles simulation: ideas, illustrations and the CASTEP code. J. Phys. Condens. Matter **14,** 2717–2743 (2002).
50. Perdew, J.P., Burke, K., Ernzerhof, M.: Generalized gradient approximation made simple. Phys. Rev. Lett. **77**, 3865 (1996).
51. Ceperley, D.M., Alder, M.: Ground State of the Electron Gas by a Stochastic Method. Phys. Rev. Lett. **45**, 566–569 (1980).
52. Perdew, P., Zunger A., Self-interaction correction to density-functional approximations for many-electron systems. Phys. Rev. B **23,** 5048–5079 (1981).
53. Vanderbilt, D.: Soft self-consistent pseudopotentials in a generalized eigenvalue formalism. Phys. Rev. B **41**, 7892 (1990).
54. Fischer, T.H., Almlof, J.: General methods for geometry and wave function optimization. J. Phys. Chem. **96,** 9768–9774 (1992).
55. Sofo, J.O., Chaudhari, A.S., Barber, G.D., Graphane: A two-dimensional hydrocarbon Phys. Rev. B **75**, 153401 (2007).

56. Sahin, H., Topsakal, M., Ciraci, S.: Structures of fluorinated graphene and their signatures. Phys. Rev. B **83**, 115432 (2011).
57. Sahin, H., Ataca, C., Ciraci, S.: Electronic and magnetic properties of graphane nanoribbons. Phys. Rev. B **81**, 205417 (2010).
58. Segall, M.D., Shah, R., Pickard, C.J., Payne, M.C.: Phys. Rev. B **54**, 16317–16320 (1996).
59. Momida, H., Hamada, T., Takagi, Y., Yamamoto, T., Uda, T., Ohno, T.: Dielectric constants of amorphous hafnium aluminates: First-principles study. Phys. Rev. B **75**, 195105 (2007).
60. Kronig, R. de L.: On the Theory of Dispersion of X-Rays. J. Opt. Soc. Am. **12**,547–557 (1926).
61. Penn, D.R.: Wave-number-dependent dielectric function of semiconductors. Phys. Rev. B 128, 2093 (1962)
62. John R., Merlin B.: Optical properties of graphene, silicene, germanene, and stanene from IR to far UV – A first-principles study. J. Phys. Chem. of Sol. **110**, 307 (2017).

Figure captions

Fig. 1 The pictorial representation of (a) C-configuration (b) B-configuration hydrogenated silicene in which white circles are indicated by hydrogen atoms and yellow circles by silicon atoms.

Fig. 2 (a) The band structure of C- configuration (b) B-configuration of hydrogenated silicene.

Fig. 3 The total density of states (TDOS) and partial density of states (PDOS) for (a) C- and (b) B- configurations of hydrogenated silicene.

Fig. 4 The calculated imaginary part of dielectric function $\varepsilon_2(\omega)$ under different pressures (a) parallel polarization (b) perpendicular polarization of electric field for C- and B- configurations of hydrogenated silicene.

Fig. 5 The real part of dielectric function $\varepsilon_1(\omega)$ under different pressures. (a) parallel polarization and (b) perpendicular polarization of electric field for C- and B- configurations of hydrogenated silicene.

Fig. 6 The refractive index $n(\omega)$ under different pressures. (a) parallel polarization (b) perpendicular polarization of electric field for C- and B- configurations of hydrogenated silicene.

Fig. 7 The birefringence for C-, B- configurations of hydrogenated silicene under different pressures.

Fig. 8 The electron energy loss function $L(\omega)$ of hydrogenated silicene under different pressures. (a) parallel polarization (b) perpendicular polarization of the electric field for C- and B- configurations.

Figures

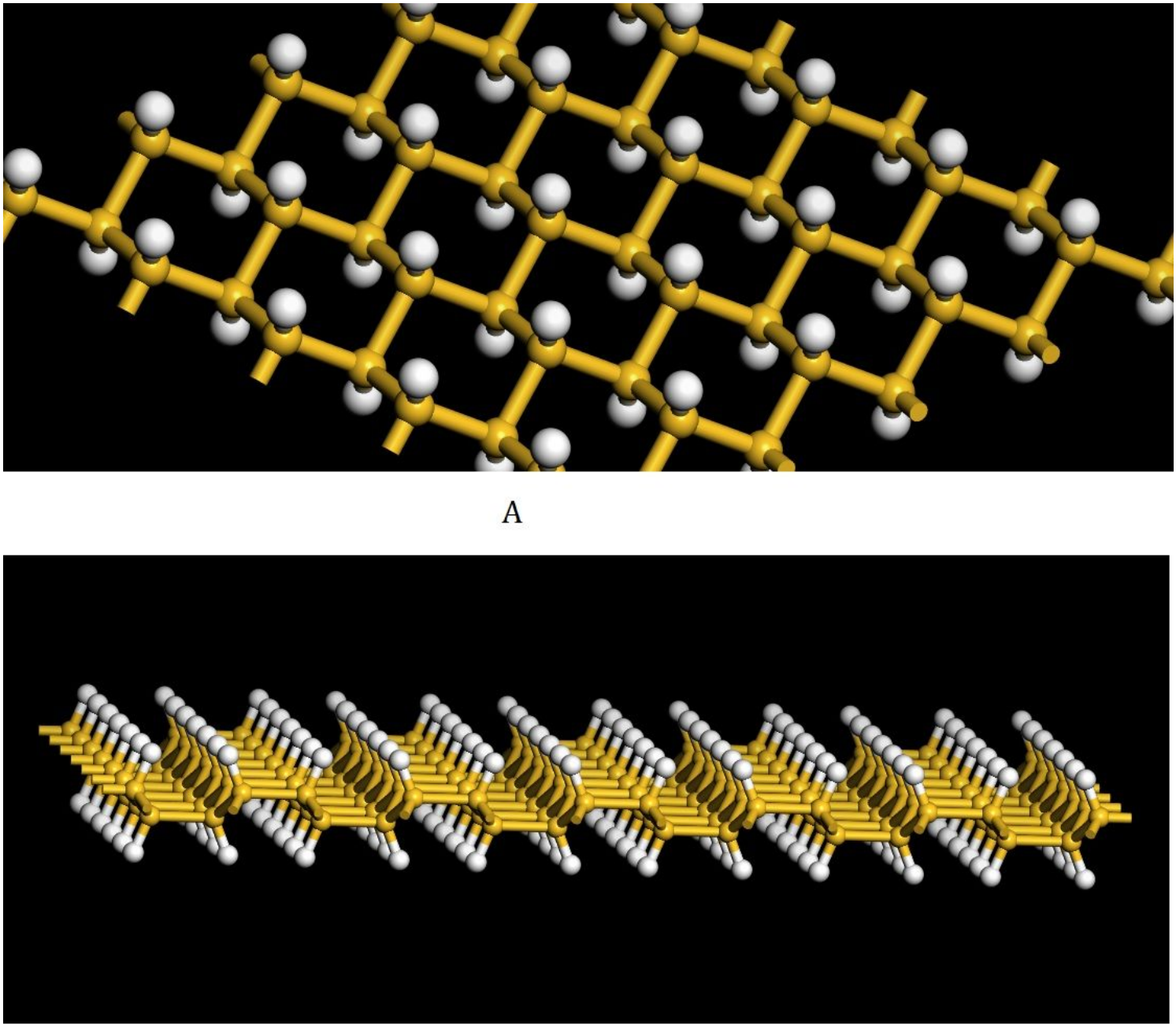

Figure 1

The pictorial representation of (a) C-configuration (b) B-configuration hydrogenated silicene in which white circles are indicated by hydrogen atoms and yellow circles by silicon atoms.

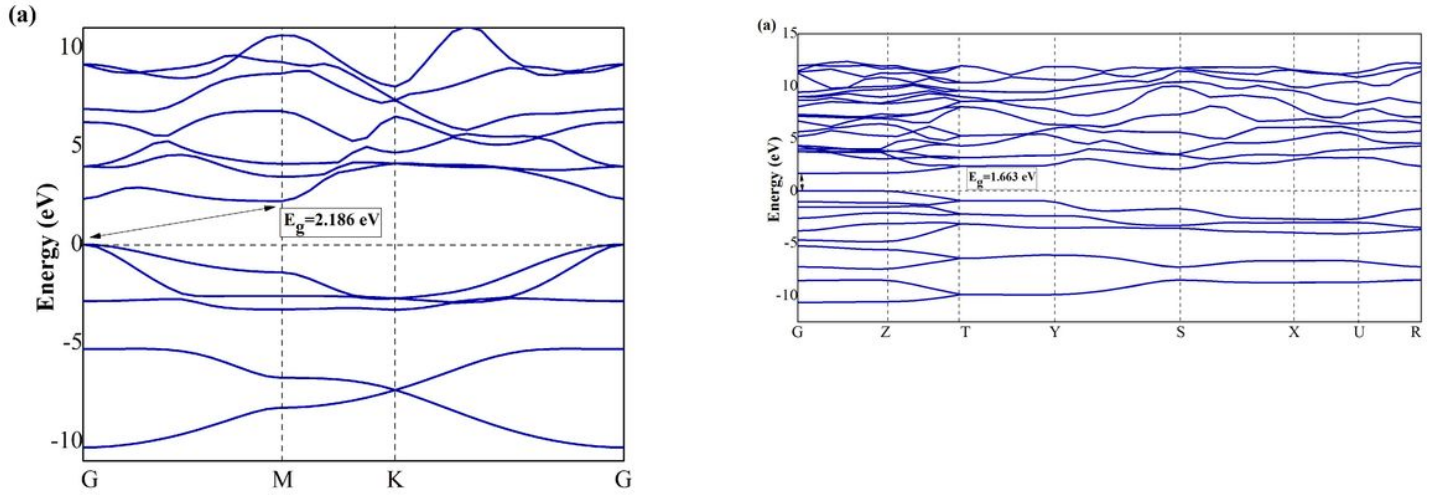

Figure 2

(a) The band structure of C- configuration (b) B-configuration of hydrogenated silicene.

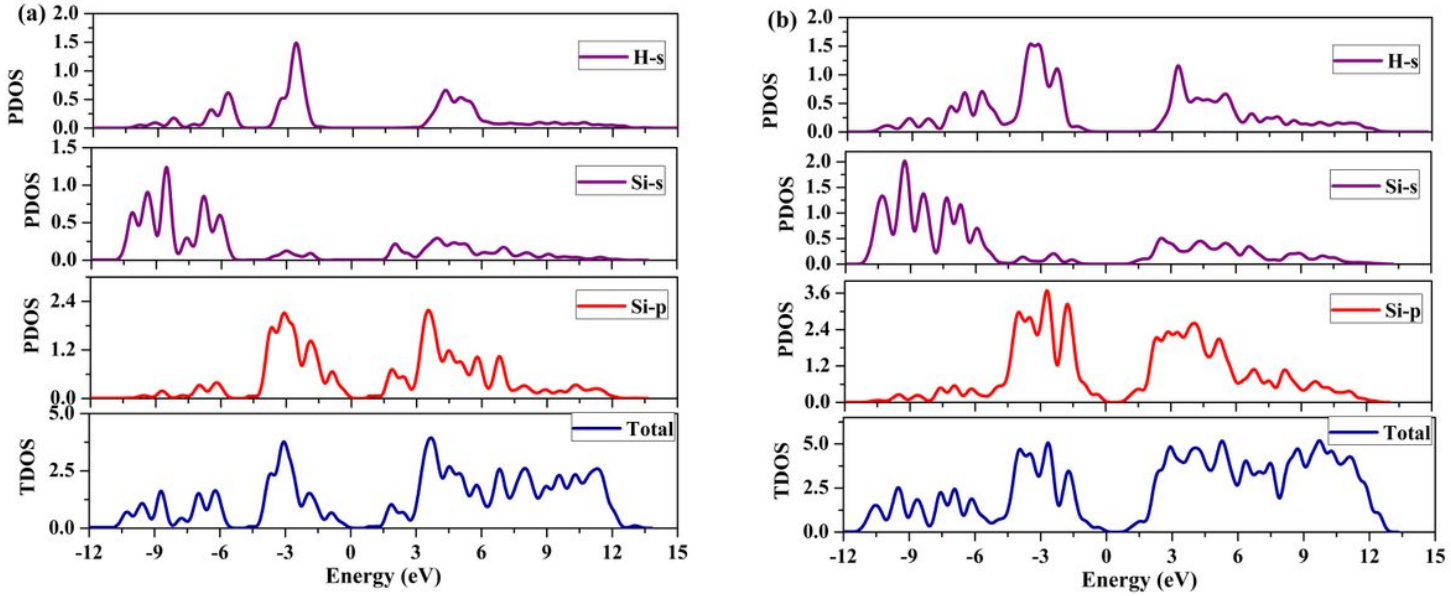

Figure 3

The total density of states (TDOS) and partial density of states (PDOS) for (a) C- and (b) B-configurations of hydrogenated silicene.

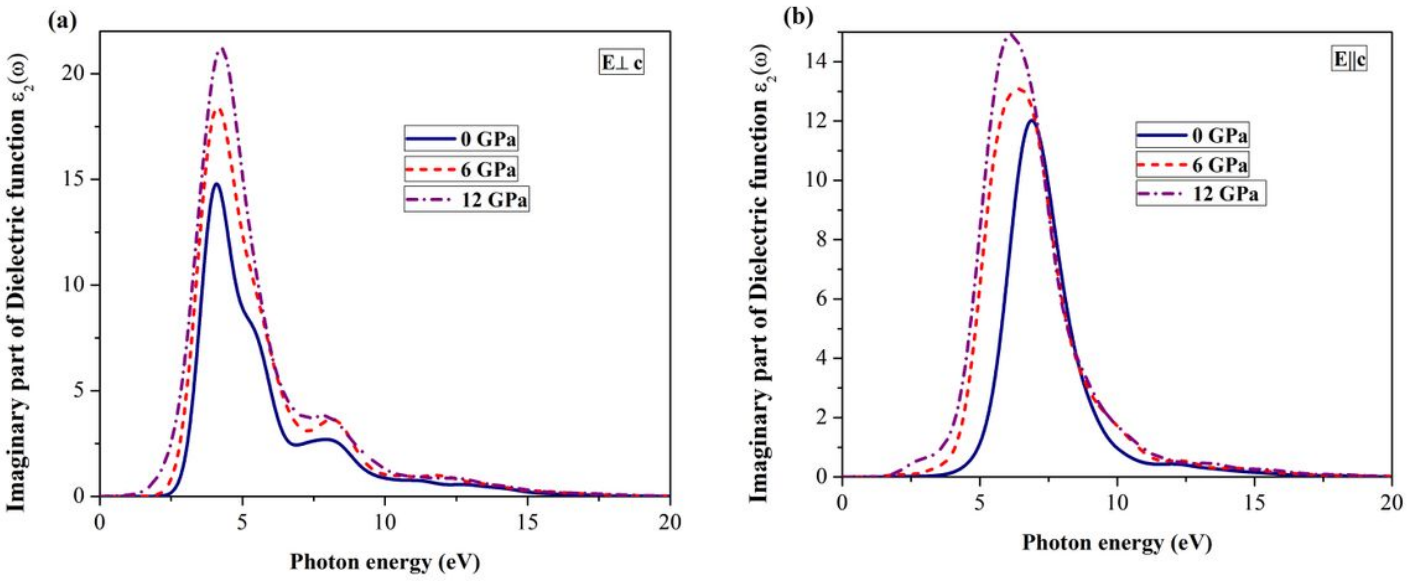

Figure 4

The calculated imaginary part of dielectric function ε2(ω) under different pressures (a) parallel polarization (b) perpendicular polarization of electric field for C- and B- configurations of hydrogenated silicene.

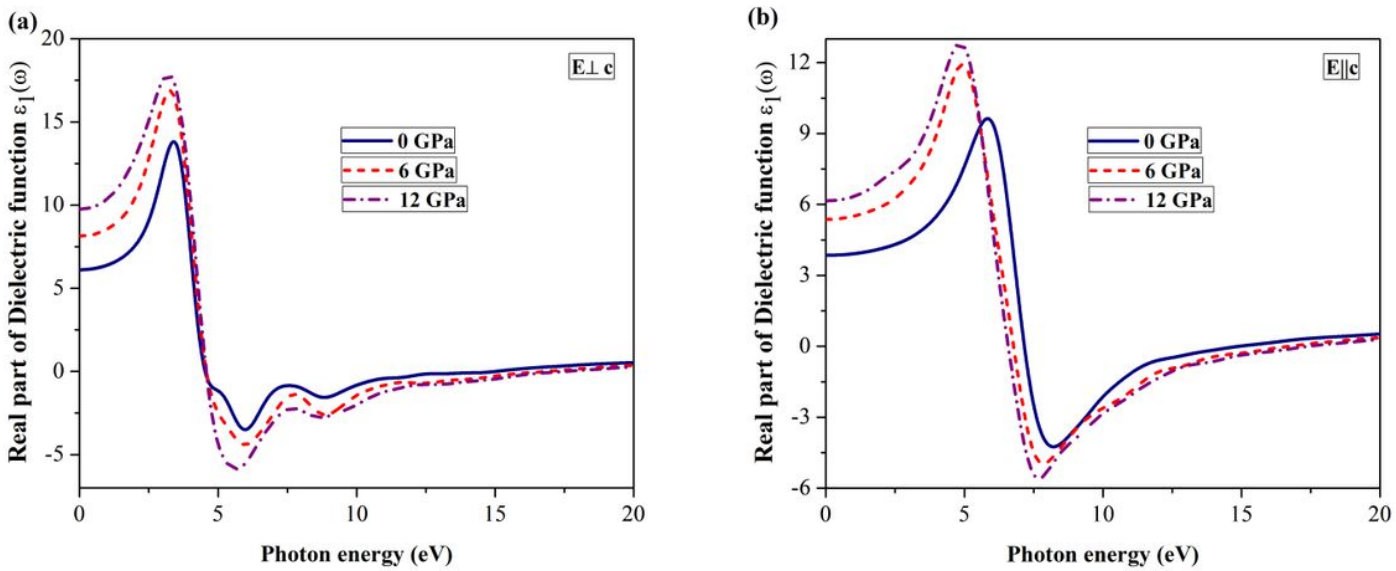

Figure 5

The real part of dielectric function ε1(ω) under different pressures. (a) parallel polarization and (b) perpendicular polarization of electric field for C- and B- configurations of hydrogenated silicene.

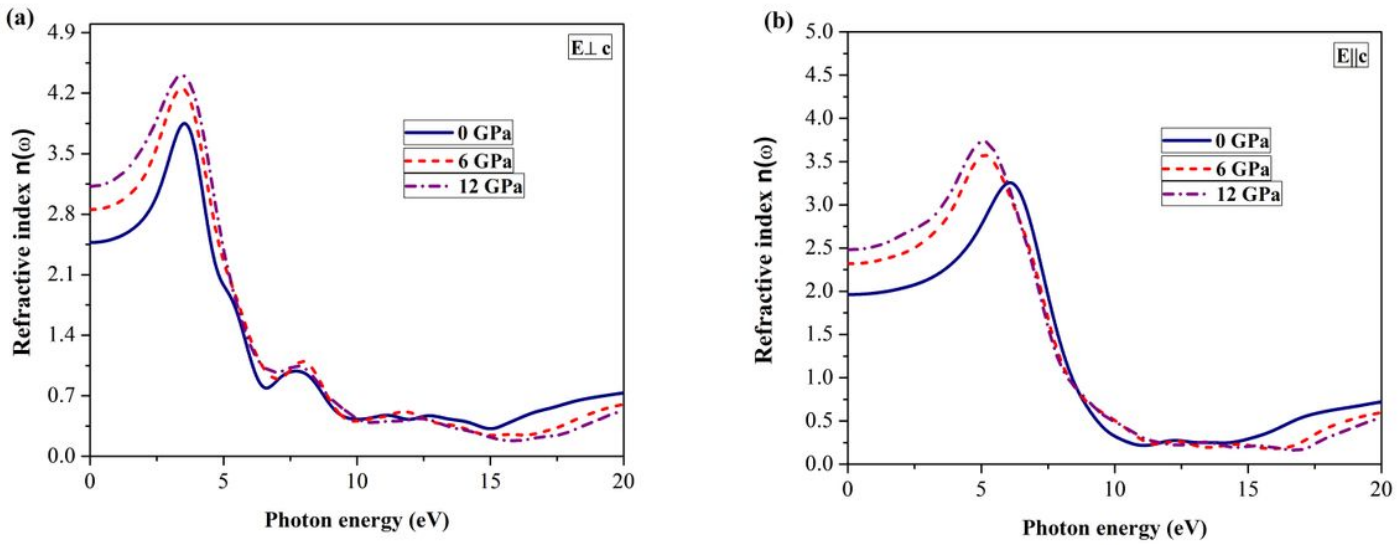

Figure 6

The refractive index n(ω) under different pressures. (a) parallel polarization (b) perpendicular polarization of electric field for C- and B- configurations of hydrogenated silicene.

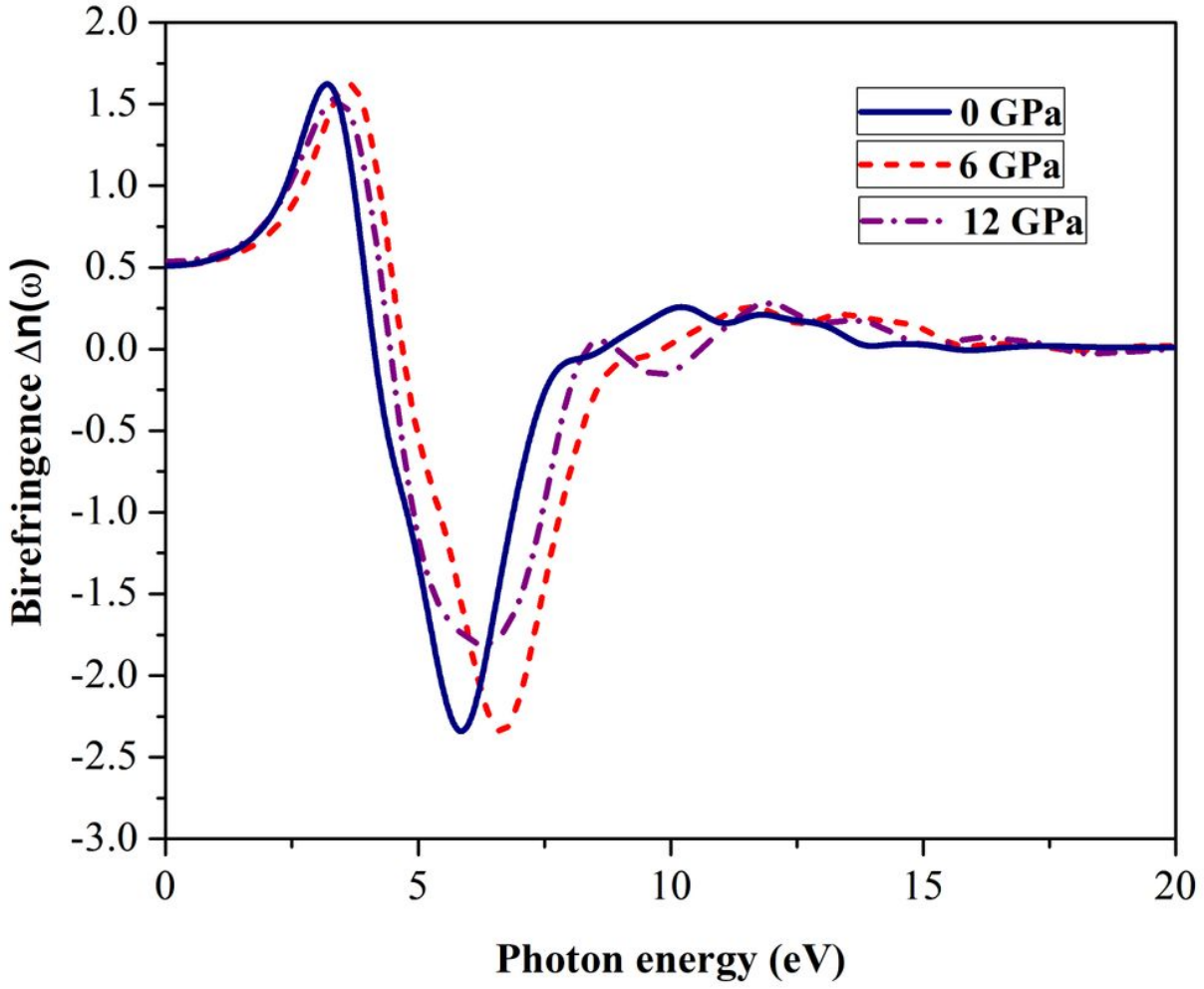

Figure 7

The birefringence for C-, B- configurations of hydrogenated silicene under different pressures.

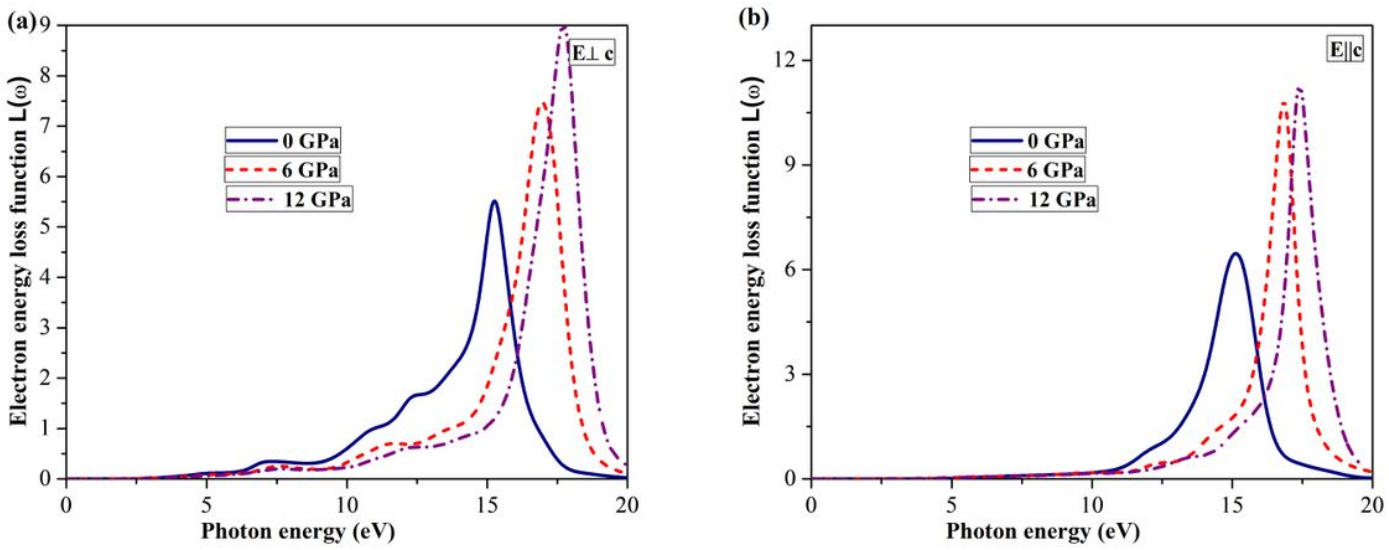

Figure 8

The electron energy loss function L(ω) of hydrogenated silicene under different pressures. (a) parallel polarization (b) perpendicular polarization of the electric field for C- and B- configurations.